World Academy of Science, Engineering and Technology
International Journal of Biomedical and Biological Engineering
Vol:9, No:6, 2015

Riemannian Manifolds for Brain Extraction on Multi-modal Resonance Magnetic Images

Mohamed Gouskir, Belaid Bouikhalene, Hicham Aissaoui, Benachir Elhadadi

Abstract—In this paper, we present an application of Riemannian geometry for processing non-Euclidean image data. We consider the image as residing in a Riemannian manifold, for developing a new method to brain edge detection and brain extraction. Automating this process is a challenge due to the high diversity in appearance brain tissue, among different patients and sequences.

The main contribution, in this paper, is the use of an edge-based anisotropic diffusion tensor for the segmentation task by integrating both image edge geometry and Riemannian manifold (geodesic, metric tensor) to regularize the convergence contour and extract complex anatomical structures. We check the accuracy of the segmentation results on simulated brain MRI scans of single T1-weighted, T2-weighted and Proton Density sequences. We validate our approach using two different databases: BrainWeb database, and MRI Multiple sclerosis Database (MRI MS DB). We have compared, qualitatively and quantitatively, our approach with the well-known brain extraction algorithms. We show that using a Riemannian manifolds to medical image analysis improves the efficient results to brain extraction, in real time, outperforming the results of the standard techniques.

Keywords—Riemannian manifolds, Riemannian Tensor, Brain Segmentation, Non-Euclidean data, Brain Extraction.

I. Introduction

NOWADAYS, the analysis of medical images has drawn the attention of several researchers, institutes, associations and organizations to fight against the incurable diseases and address the problem of the increasing number of images and diagnosis time, to be able develop systems for automatic detection and classification. Since the brain extraction offers a significant step for the diagnosis of medical images. We propose, in this paper, to present an application of Riemannian manifolds to such a technique.

For an Accurate computer-aided diagnosis of magnetic resonance imaging of the human brain, the extraction of brain regions is a very important step for most methods and image analysis techniques. This step is to exclude all external brain tissues, such as the skull, dura, eyes, etc, with precision, without touching any part of the brain tissue. However, the increase in number of the images acquired every day in hospitals and medical centers requires the development of methods for automatic analysis of multi-sequence information to aid diagnosis.

Medical imaging has recently known the development of new modalities, which has made the analysis of images very complex, thus, such images are not scalar values. This progression in the image data processing is not in Euclidean space, but can be found in Riemannian manifolds.

Mathematically speaking, using non-Euclidean image data a differential manifolds can be modeled. On a manifold, geometric quantities are measured using Riemannian metric [1]. The image data are considered as residing in a Riemannian manifold and are represented in the exponential map for this manifold together with the Riemannian weighted mean of image data [2]. The segmentation of brain tissues, of both low and high grades, using supervised method, based on a Riemannian manifold. It starts with a pre-processing step, after that the features are extracted and each pixel is classified. Finally, a post-processing step is applied to the classified pixel, and the provided analysis includes T1, T2, FLAIR and T1 with contrast (T1C).

A. Related Works

Image analysis using the differentiable geometry become a very important area for non-Euclidean data. The use of Riemannian geometry is more common for medical image processing, in particular, and forms processing, in general. In computer vision, the Riemannian geometry is used for the geometry of 2D and 3D objects, which are invariant to rotation, translation and scaling. The Riemannian manifolds are used also for different processing phases of forms. The symmetric positive definite matrix (tensor) is used in the image filter [3], [1], in edge detection based geodesic distance and Riemannian metrics [4], [5], [6], in segmentation and texture analysis [7], [8], [9], [10], [11], and in classification [11], [12], has a natural structure as a Riemannian manifold. In this respect, various applications are presented. To robust atlas estimation the geometric median on Riemannian manifolds is used as a minimizer of the sum of geodesic distances which provides a robust statistical estimator of centrality for manifold-valued data, [13] developed the concept of median geometry to general Riemannian manifolds.

Riemannian manifolds have also shown their effectiveness in the human re-identification used by [6] to distinguish sets of patches belonging to specific individuals. The works of [12] aim to extend the definition of the Ricci calculus to the case of high angular resolution of diffusion tensor using a Riemannian scalar measure for tensor valued image analysis. Based on the tensor clustering methods [7], the extraction of the neural tracts of interest from a diffusion tensor image and the delimitation of the border of bundle, by the combined algorithms of connectivity maps and tensor distances. Recently, [14] has used an anisotropic diffusion tensor for extracting the local

Mohamed Gouskir, Hicham Aissaoui and Benachir Elhadadi are with the Laboratory of Sustainable Development, Faculty of Science and Techniques, Sultan Moulay Slimane University, Beni Mellal, Morocco (e-mail: m.gouskir@usms.ma).

Belaid Bouikhalene is with the Laboratory for Interdisciplinary Research in Science and Techniques, Polydisciplinary Faculty, Sultan Moulay Slimane University, Beni Mellal, Morocco.

information for edge detection and segmentation of brain tumor [11].

We now present a brief overview on publications dealing with segmentation and extraction of brain and diffusion tensor data. Brain extraction, also known as skull stripping, is one of the most important preprocessing steps for automatic brain image analysis, several approach and techniques to perform brain segmentation and extraction is proposed. Starting with the brain extraction algorithm (BEA) for T2-weighted magnetic resonance imaging (MRI) scans [15] based on low pass filter to remove background, morphological operations and largest connected component to obtain the brain mask from which the brain is extracted. The authors proposed in [16] the brain extraction method for T1-weighted MRI, using region labelling and morphological operations, and adaptive intensity thresholding method. Nonlocal segmentation technique embedded in a multi-resolution framework [17], applied on a large dataset. The brain extraction from T2-weighted MRI was done using histogram based gradient calculation by [18]. The primary brain areas; gray matter (GM), white matter (WM), and cerebrospinal Fluid (CSF) were extracted efficiently out from 2D to 3D images. Hidden Markov model and graph cuts methods were used to brain segmentation by [19], [20], respectively. One more method is the adaptive region growing algorithm developed by [21] to evolve a front at the seed region of interest (ROI) based on a region growing algorithm which uses the complementary information provided by conventional MRI, such as T1 weighted and T2-weighted to perform the brain segmentation and extraction.

Despite all these efforts, all of these algorithms present limitations and issues to be solved for a consistent and efficient brain extraction algorithm. BET and BSE [22], [23] include regions outside the brain into the brain tissues [21], these algorithms present also bad results in poor spatial resolution and noisy images, BET does not always give satisfactory results on 3D-T1 images and time-consuming [24]. On the other hand, approaches require one slice like [25] and the others require the images being T1-weighted or t2-weighted [15], [16], it makes a hard constraint in clinical routine applications.

In this paper, we extend the Riemannian manifolds approaches to perform the automatic extraction of brain regions on multi-modal RMI T1-weighted, T2-weighted and Proton Density images captured in tree views coronal, sagittal and axial. We demonstrate the validity of this approach with a qualitative and quantitative result using two different data sets: Brainweb database and MRI Multiple sclerosis database. The obtained results show an efficient performance in different modalities compared with previous methods.

B. Our Contributions

The main contributions of our study may be summarized as:

- We propose a brain extraction algorithm based on the Riemannian manifold relying on the works cited on the previous subsection and on the problems encountered in some methods.
- Supposing that an MR image is residing in non-Euclidean data, we firstly, propose an efficient smoothing for MRI data extended from Riemannian geometry, than we refer to the metric tensor for brain segmentation to obtain a brain mask.
- Our method is inspired from the metric tensor, which is based on the geodesic distance and the edge detection proposed by [1], [2] and [7]. Such an algorithm is, then, generalized to extracting brain regions.

II. Theory

A. Riemannian Differential Geometry

We review some basic definitions and notations in Riemannian geometry. Given any point $p \in M$ and a tangent vector $\xi \in T_pM$, the tangent space of M at p, M is a differentiable manifold in the vicinity of p. There is a maximal open interval $I_\xi \in \mathbb{R}$ about the origin and an unique geodesic curve $\gamma_\xi \in M$ satisfying $\gamma_\xi(0) = p$, $\gamma'_\xi(0) = \xi$ (Fig. 2). The map $\gamma : \Omega \to M$ where $t \to \gamma(t)$ is a path, the vector field along γ is defined if the affine connection $\nabla_{\dot\gamma}\xi = 0$. Let U be an open set in $\mathbb{R}^n$, and let P and Q be smooth vector fields on U. Then:

$$P = \sum_{i=1}^{n} a^i \frac{\partial}{\partial x^i}, \qquad Q = \sum_{i=1}^{n} b^i \frac{\partial}{\partial x^i}$$

where $a^1, a^2, ..., a^n$ and $b^1, b^2, ..., b^n$ are the components of the vector fields P and Q with respect to the Cartesian coordinate system $(x^1, x^2, ..., x^n)$ on $\mathbb{R}^n$. The directional derivative $\partial_P Q$ of the vector field Q along the vector field P is then given by the formula:

$$\partial_P Q = \sum_{i,j=1}^{n} a^j \frac{\partial b^i}{\partial x^j} \frac{\partial}{\partial x^i} \tag{1}$$

From (1), since the connection ∇ is torsion-free, we can demonstrate that:

$$\partial_P Q - \partial_Q P = \nabla_P Q - \nabla_Q P = [P, Q] \tag{2}$$

Then the differential operator, sending smooth vector fields p and Q to $\partial_P Q$, is an affine connection on U. For the given map $(U, x^1, x^2, ..., x^m)$, we put:

$$\nabla_{\partial_i}(\partial_j) = \Gamma_{ij}^k \partial_k$$

In a system of local coordinates given with $P = \xi^i \frac{\partial}{\partial x^i}$ and $\dot\gamma = \frac{dx^i}{dt}\frac{\partial}{\partial x^i}$ we have.

$$\nabla_{\dot\gamma} P = \left(\frac{d\xi^i}{dt} + \Gamma_{jk}^i \xi^k \frac{dx^i}{dt}\right)\frac{\partial}{\partial x^i}. \tag{3}$$

This shows that $\nabla_{\dot\gamma} P$ depends only on the values of P along the curve γ.

The exponential map defined in tangent space to manifolds $exp_p : T_p(M) \to M$ by $exp_p(\xi) = \gamma\xi$, thus the curve $\gamma_\xi(t) = exp_p(t\xi)$. Since the exponential map exp_p is a local diffeomorphism, it has an inverse map so-called logarithmic map $log_p : M \to T_pM$ where $log_p(\gamma_\xi(t)) = t\xi$.

Now we briefly mention the notions involving cut points. Let $E_p = \{\xi \in T_p(M) \setminus \|\xi\| = 1\}$. For each $\xi \in E_p$ we

define $C(\xi) = sup\{t > 0 \ : \ d(p, \gamma_\xi(t)) = t\}$, Where d is the Riemannian distance.

For t sufficiently small, the point $exp_x(t\xi)$ has the normal coordinates $x^i = \xi^i t$, $\xi = \xi^i e_i$. However, $exp_x(t\xi) = \gamma_\xi(t)$ is the geodesic with initial velocity ξ.

$$0 = \Gamma^i_{jk}(t\xi^1, ..., t\xi^m)\xi^j\xi^k.$$

At $t = 0$, $0 = \Gamma^i_{jk}(0)\xi^j\xi^k$ for any choice of $(\xi^1, ..., \xi^m)$, which demonstrates

$$\frac{d\xi^i}{dt} + \Gamma^i_{jk}\xi^k\frac{dx^j}{dt} = 0.$$

The vector field along γ in the initial condition. The geodesic distance along the curve γ is defined as:

$$\nabla_{\dot\gamma}\gamma = 0 \tag{4}$$

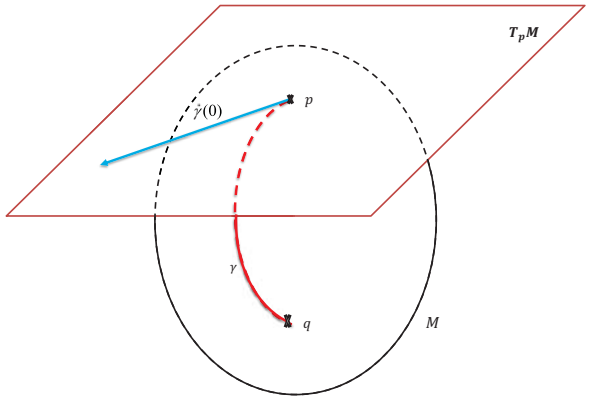

Fig. 1 The geodesic curve $\gamma(t)$ defined by the starting point P and the initial velocity $\gamma'(0)$. The endpoint is computed by applying the exponential map, such that $q = exp_p(\gamma'(0))$ [10]

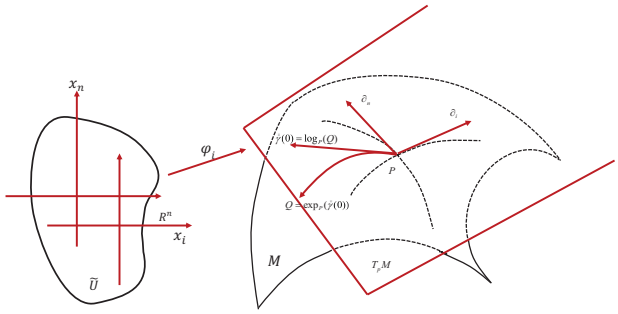

Fig. 2 Local coordinate system, geodesic curve $\gamma(t)$,tangent space and exponential map at $p \in M$ [10]

B. The Space of Diffusion Tensor

Let x be a point of the manifold that we consider as a local reference and $\overrightarrow{xy}$ a vector of the tangent space T_xM at that point. The function of exponential map, defined in the tangent space T_xM, can maps to each vector $\overrightarrow{xy} \in T_xM$ the point y of the manifold by the geodesic starting from x. There exists one and only one geodesic starting from that point with this tangent vector.

In Riemannian manifolds, we denote the logarithmic map, $\overrightarrow{xy} = log_x(y)$, as the inverse of the exponential map, $y = \exp_x(\overrightarrow{xy})$. Let $S(n)$ be the space of $n \times n$ symmetric matrices and $S^+(n)$ the space of symmetric positive-definite matrices. A real $n \times n$ matrix M is symmetric if $M = M^T$ and positive definite if $x^T Mx > 0$ for all nonzero $x \in \mathbb{R}^n$, we consider an a diffusion tensor MRI as tensor, is also a differentiable manifold with a natural Riemannian structure. Moreover, can formulated as a Riemannian symmetric space. Which lead to computing geodesics along curves. The forms of different operators (metric, tensor, connection, geodesics, ...) depend on the Riemannian manifold and metric. The feature space of diffusion tensor of MRI is identified with $S^+(3)$. At each point $p \in S^+(n)$, the identity mapping $p \in S^+(n) \to (\sigma_{11}, ..., \sigma_{ij}), i \le j, i, j = 1, ..., n$, the tangent space $T_pS^+(n)$ is equal to $S(n)$. So a basis of $T_pS^+(n)$ can be defined as:

$$\frac{\partial}{\partial\sigma_{ij}} \leftrightarrow E_{ij} \in S(n), i \le j, i, j = 1, ..., n \tag{5}$$

where,

$$E_{ij} = \begin{cases} 1_{ij} & Si \ \ i = j. \\ 1_{ij} + 1_{ji} & Si \ \ i \neq j. \end{cases} \tag{6}$$

and 1_{ij} is the $n \times n$ matrix with 1 at element (i, j) and 0 everywhere else. to convert $S^+(n)$ into a Riemannian manifold, one can introducing a Riemannian metric g at point p.

$$g(\frac{\partial}{\partial\sigma_{ij}}, \frac{\partial}{\partial\sigma_{kl}}) = \langle\frac{\partial}{\partial\sigma_{ij}}, \frac{\partial}{\partial\sigma_{kl}}\rangle_p = tr(p^{-1}E_{ij}p^{-1}E_{kl}). \tag{7}$$

where $tr(.)$ denotes the trace, The positive-definite inner product can be written as $\langle A, B\rangle_p = tr(p^{-1}Ap^{-1}B)$, $A, B \in T_pS^+(n)$ [1], [2], [26]. The geodesic distance between two point $A, B \in S^+(n)$ is the minimum length of curves connecting them, e.g. $d_g(a, b) = argmin_C\{l(C)|C(a) = A, C(b) = B\}$ for a smooth curve $C(t) : [a, b] \to S^+(n)$ in $S^+(n)$, the length of $C(t)$ can be computed as:

$$l(C) = \int_a^b \|C'(t)\|_{C(t)}dt = \int_a^b \sqrt{tr(C(t)^{-1}C'(t))^2}dt. \tag{8}$$

The geodesic with the initial point and tangent vector $\Sigma \in T_IS^+(n)$ given by $exp(t\Sigma)$, I is the identity matrix. An arbitrary geodesic $\gamma(t)$ such that $\gamma(0) = p$ and $\gamma'(0) = \Sigma$, under the group action [26], is given by:

$$\gamma_{(p,\Sigma)}(t) = p^{1/2}\exp(tp^{1/2}\Sigma p^{-1/2})p^{1/2}. \tag{9}$$

From (9), it follows that $exp_p(\Sigma) = p^{1/2}\exp(p^{1/2}\Sigma p^{-1/2})p^{1/2}$. The logarithmic map is given by $log_p : S^+(n) \to T_pS^+(n)$ o $log_p(\gamma_{(p,\Sigma)}(t)) = t\Sigma$. Therefore, for a point A near p

$$log_p(\Sigma) = p^{1/2}\log(p^{-1/2}Ap^{1/2})p^{1/2} = p\log(p^{-1}A). \tag{10}$$

Thus, the geodesic distance between two points x and y in $S^+(n)$, using the Frobenius norm of a matrix ($\|.\|_F$) is given by:

$$d(x,y) = \left\|\log(x^{-1}y)\right\|_F = \sqrt{tr[\log(x^{-1}y)^T.\log(x^{-1}y)]}. \quad (11)$$

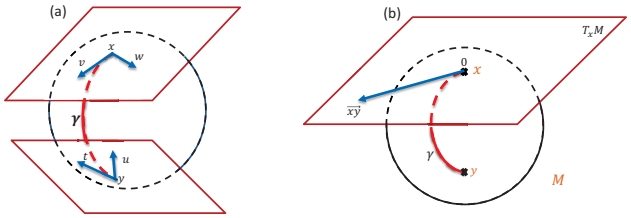

Fig. 3 (a): The tangent planes at points x and y of the sphere S_2 are different: the vectors v and w of T_xM cannot be compared to the vectors t and u of T_yM. (b): The geodesics starting at x are straight lines in the exponential map and the distance along them is conserved [2].

C. Nonlinear Diffusion Filtering Generalised

In this section, we use an anisotropic Gaussian kernel for image smoothing and filtering to obtain an efficient edge detection of brain images. The application of Anisotropic Diffusion to digital images processing, comes from the application of the equation of heat diffusion to evolve gray-scale images $f(x,y)$. The Ficks low giving the expression of the flux j by the following equation:

$$\mathrm{j} = -\mathrm{U}.\nabla \mathrm{f} \quad (12)$$

where, ∇f is the gradient. The relation between ∇f and j is described by a positive-definite, symmetric matrix U referred to as diffusion tensor. The local variation the overall energy in the image is driven by $\frac{\partial \mathrm{f}}{\partial \mathrm{t}} = -\mathrm{div(j)}$. The PeronaMalik Anisotropic Diffusion use the following anisotropic diffusion equation to evolve gray-scale images $f(x,y)$.

$$\frac{\partial \mathrm{f}}{\partial \mathrm{t}} = -\mathrm{div}(\mathrm{U}.\nabla \mathrm{f}) \quad (13)$$

Expresses the variation of energy at every position in the image, where $\mathrm{U} = \rho(\|\nabla f\|^2)$ is a scalar function of the gradient of image f, and the function ρ is an edge-stopping, halt the heat-ow process at object boundaries. This idea is to measure the conductivity of the image depending upon the Euclidean magnitude of the gradient. However, they propose a simpler, discrete scheme based on the transfer of energy between each pixel and its four direct neighbors. First, we define an anisotropic Gaussian kernel for smoothing MR images. Gaussian smoothing calculates weighted averages in an image region. The classical Gaussian filter has been generalized by [1] and [2] to smooth non-linear image data, e.g. tensor-valued images.

$$G_{\sigma_x}(x) = \frac{1}{(\sqrt{2\pi}\sigma_x)^n}.\exp(-\frac{x^T x}{2\sigma_x^2}) \quad (14)$$

The smooth image is $f_{\sigma_x}(x) = G_{\sigma_x} * f_0$, where G_σ represents a Gaussian filter with standard deviation σ and $*$ is the convolution operator. We suppose a neighbouring window contains the pixel set $x_1, ..., x_m$ that is $f_{\sigma_x}(x) = \sum_{k=1}^{m} G_{\sigma_x}(x_k)p_k$. At position x the Riemannian filter outputs the Riemannian weighted mean for the feature set:

$$f_{Gausmo} = \arg\min_{p\in M}(\frac{1}{2}\sum_{k=1}^{m} G_{\sigma_x}(x_k)d_g(p, f_0(x_k))^2). \quad (15)$$

The degree of smoothing can be controlled by the filter width σ_x of the Gaussian kernel. The performance of the Riemannian filter can be automatically adapted to the noise distribution of the image. If the impulse noise dominates the local region of a pixel, then the filter performs predominately like a median filter and it is more likely to output one of the neighbouring data-values.

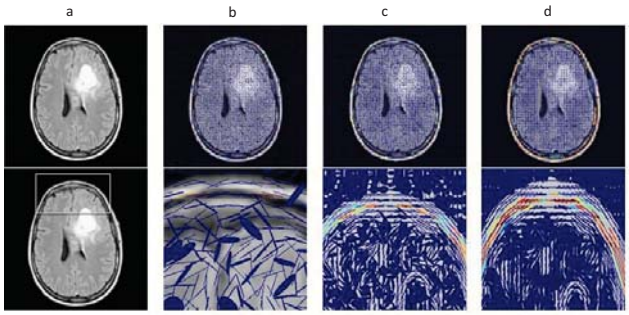

Fig. 4 Examples of brain region delimitation for medical images using anisotropic diffusion generalized as non-Euclidean image data for different deviation. The first line shows the results of the algorithm on the image, the second line shows the results of the game frame for different values of σ. (b), (c) and (d) for 0.5, 2 and 4, respectively

III. Brain Detection Based on Structure Tensor

The structure tensor is a field of symmetric positive matrices that encodes the local orientation and anisotropy of an image. In this section, we show how to a structure tensor will be generalized and applied to the MRI brain detection as non-Euclidean image.

Based on [1] which generalized the structure tensor to non-Euclidean image data and on [27], [26], the image data can be considered as a map domain from Ω in a differentiable manifold M. i.e. $f : \Omega \in \mathbb{R}^2 \to M$. The local variation of a 2-dimensional image f, noted df, is given by

$$df = \frac{\partial f}{\partial x_1}dx_1 + \frac{\partial f}{\partial x_2}dx_2.$$

The square vector norm is:

$$df^2 = \sum_{i=1}^{2}\sum_{j}^{2}(\frac{\partial f}{\partial x_i}.\frac{\partial f}{\partial x_j})dx_i dx_j \quad (16)$$

where $\partial f/\partial x_i$ is the directional derivative of f along x_i. Such that $h_{ij} = \frac{\partial f}{\partial x_i}.\frac{\partial f}{\partial x_j}$, define the metric tensor, we have $df^2 =$

$dx^T h dx$ where $dx = (dx_1, dx_2)^T$. Now we consider an image f as a 2-dimensional manifold M_r in M, the parametrisation $\Phi : M_r \to M$, $\partial f/\partial x_i$ is a basis of $T_x M_r$. Let x_1, x_2 be the local coordinates of M_r, then the map is given by:

$$(x_1, x_2) \to \Phi_1(x_1, x_2), ..., \Phi_n(x_1, x_2)$$

The metric tensor h measures the length of the arc ds in M_r as:

$$ds_h^2 = \sum_{i=1}^{2} \sum_{j}^{2} h_{ij} dx_i dx_j. \tag{17}$$

and the metric tensor g don M is:

$$ds_g^2 = \sum_{i=1}^{2} \sum_{j}^{2} g_{ij} d\Phi_i d\Phi_j. \tag{18}$$

We assume that Φ is isometric, then (17) and (18) are equal, and by using the rule of change coordinates. The Riemannian metric tensor h is:

$$h_{kl} = \sum_{i=1}^{2} \sum_{j=1}^{2} g_{ij} \frac{\partial \Phi_k}{\partial x_i} \frac{\partial \Phi_l}{\partial x_j}. \tag{19}$$

The metric tensor h characterizes the local geometry of image f, any change of f is stock at the unit direction $v = (dx_1, ...dx_2)$, that maximizes or minimizes df^2. The maximal and minimal rate of changes at a given point is given by the maximum λ_+ and minimum λ_-, eigenvalues of the structure tensor h, corresponding to eigenvectors e_+, e_-, which are the directions of maximal and minimal changes.

$$\begin{cases} \lambda_{\pm} = \frac{h_{11}+h_{22} \pm \sqrt{(h_{11}-h_{22})^2+4h_{12}^2}}{2} \\ e_{\pm} = (2h_{12}, h_{22} - h_{11} \pm \sqrt{(h_{11}-h_{22})^2+4h_{12}^2})^T \end{cases} \tag{20}$$

The edge detection of brain regions is controlled by the values of the eigenvalues $\lambda_{\pm}$, and eigenvectors $e_{\pm}$ of the structure tensor. When the image is scalar-valued, means that $e_+ = \nabla f / \|\nabla f\|$, $e_- = \nabla f^T / \|\nabla f\|$, $\lambda_+ = \|\nabla f\|^2$ and $\lambda_- = 0$. λ_+ and λ_- that discriminate different local geometries. The location of brain from non-brain regions is relative to the CSF that separate include and exclude regions. The CSF has a lower intensity value than the nearby brain regions and other structures. The different regions considered as different local geometries identified by the eigenvalues and eigenvectors to separate them (Fig. 4). To detect both edges and corners of brain we use the gradient norm $GN = \sqrt{\lambda_+ + \lambda_-}$ [1]. With these rules, we obtain a classification of the new voxels depending on their neighborhood with connectivity 4.

In Fig. 5 the color and aligned square delimits the seed region of interest (ROI). Each line contains an image with a different texture, and each column represents the segmentation with proposed algorithm which based on the anisotropic diffusion and structure tensor for different values of deviation σ. (a) original image, (b) segmented image for $\sigma = 0.5$, (c) for $\sigma = 2$, and (d) for $\sigma = 4$.

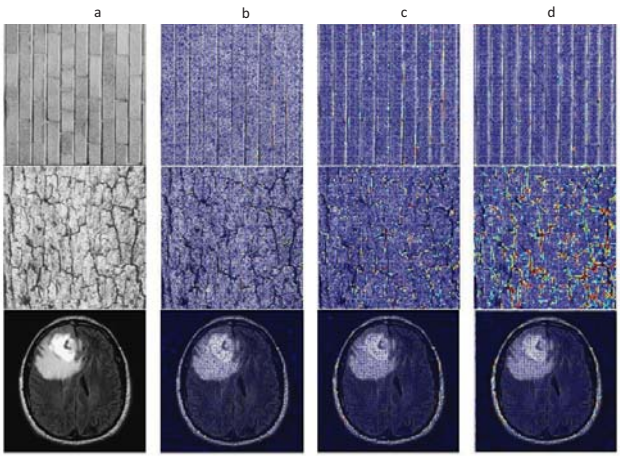

Fig. 5 Segmentation of some objects including different feature and brain MRI based on structure tensor

IV. Segmentation and Extraction of Brain MRI

Based on the proposed method, we develop a fully automatic segmentation algorithm, of 2-D brain images, for multimodal MR images. The segmentation procedures based on edge detection algorithm, as shown in Fig. 5, using the structure tensor growing as cercal on four neighbor pixels based on the eigenvalues and eigenvectors (20). The segmentation of region of interest (ROI) f_0 is based on the radius r of the tensor circles C, if the neighboring pixels have an intensity close, then the surface in which the tensor propagate belong to the ROI, Otherwise belongs to the non-brain tissues (Fig. 6 c).

$$f_0(i,j) = \begin{cases} C(i,j) & if \quad r < \varepsilon \\ 0 & Otherwise \end{cases} \tag{21}$$

We first applied the proposed algorithm for T1-weighted (T1w) MRI scans, which are most often used for brain tissue segmentation, due to the generally high WM and GM contrast and the reduced effects of WM lesions in patients with neuro-degenerative diseases, Then tested on multi-modal MR images. The proposed algorithm has tested, also, for different gray scaling texture of The USC Texture Mosaic Images dataset [28] as shown in Fig. 5. Very simple procedure will derive a boundary from a connected region of pixels, and conversely can fill a boundary to obtain a region of interest. After getting the mask of brain region using the geometric characteristics we will derive the skull from the brain image. We proceed to separate the brain from non-brain tissue. However, the proposed method exclude the background, the skull, and bone, and the brain tissue include all cerebral White Mater (WM), Gray Mater (GM) and Cerebrospinal Fluid (CSF) in ventricles and along the surface of brain and include also the tumor region.

$$f_{br}(i,j) = \begin{cases} f_0(i,j) & if \quad (i,j) \in R \\ 0 & Otherwise \end{cases} \tag{22}$$

Most methods of brain extraction are developed for T1-weighted [17], the other methods include different

sequences of magnetic resonance images, without tumor region. Our approach is to segment brain regions that contains both normal and abnormal regions, to develop a framework for detecting brain tumors based on a pre-treated image.

After the segmentation of the brain, we use the principle of region growing method for extracting the surface of the segmented brain to the different weighted of MRI, T1-weighted, T2-weighted and Proton Density in the tree main slices axial, sagittal and coronal. The proposed method shown the efficient results to brain region segmentation and extraction included the WM, GM and CSF. The qualitative and quantitative results are shown in Figs. 10, 11 and 12 regrouped, in axial slice, coronal and sagittal slice, respectively, for the three different modalities.

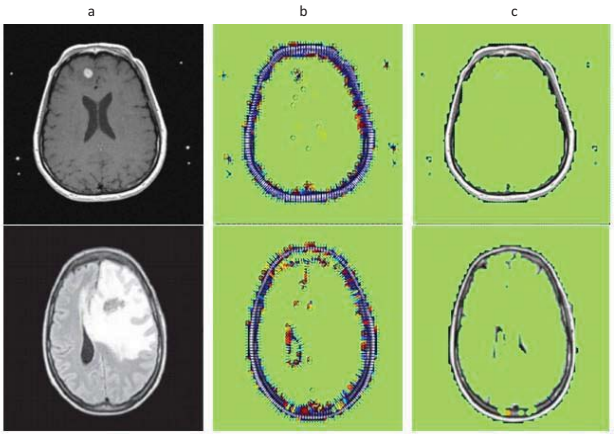

Fig. 6 The steps of the brain segmentation based on the Riemannian metric tensor from the left to right, (a) original image, (b) the smooth of the image, (c) mask of brain image based on the computation of tensors

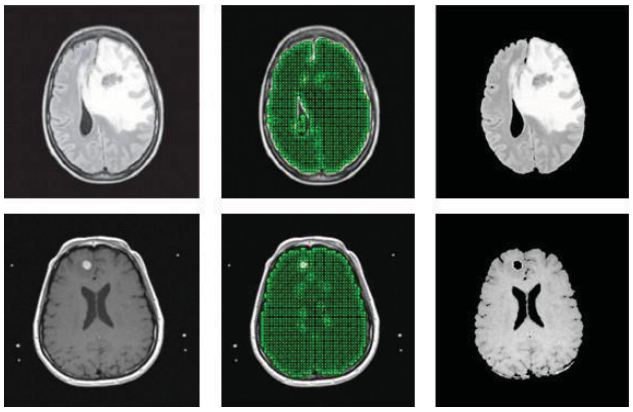

Fig. 7 Representation of brain segmentation using our algorithm, first line represent the result of T2-weighted and second line their of T1-weighted and from lift to right, the original image, brain mask based on the tensor and brain extraction using tensor growing

V. Experiments

In this section, we present the performance of our approach quantitatively and qualitatively to brain extraction, and we compare the results with the most known approach and methods cited previously or used in state of the art.

Data sets

To evaluate the performance of our approach, we use the following data sets:

1) *BrainWeb:* contains the MRI volumes for normal brain. The parameter settings are fixed to 3 modalities (T1w, T2w, and PD), 5 slice thicknesses (1mm, 3mm, 5mm, 7mm, and 9mm), 6 levels of noise (0%, 1%, 3%, 5% 7% and 9%), and 3 levels of intensity non-uniformity (0%, 20%, and 40%). The discrete anatomical model applied to generate the simulated brain MRI data was used as ground truth data. The discrete anatomical and the simulated brains were transformed to coronal and sagittal slices before starting the experiments.
2) *MRI Multiple sclerosis Database (MRI MS DB):* Thirty-eight patients (17 males, and 21 females), aged 34.1 ± 10.5 (mean age $\pm$ standard deviation), with a CIS of MS and MRI-detectable brain lesions were scanned twice at 1.5 T with an interval of 6-12 months. The transverse MR images used for the analysis were obtained using a T2-weighted turbo spin echo pulse sequence (repetition time=4408 ms, echo time=100ms, echo spacing = 10.8 ms). The reconstructed image had a slice thickness of 5 mm and a field of view of 230 mm with a pixel resolution of 2.226 pixels/mm. Standardized planning procedures were followed during each MRI examination [29], [30].

To validate qualitatively the obtained results with ground-truth masks, we use the Dice Similarity Coefficient (DSC)[31]. This measure indicates the amount of area overlap between the automatically detected and the manually delineated brain image. This measure is calculated as follows:

$$DSC = \frac{2 \times TP}{2 \times TP + FP + FN} \tag{23}$$

where TP (True Positive) are the correct detections, FP (False Positive) are incorrect detections, and FN (False Negative) are missing detections. The performance of our implementation is qualitatively shown in Fig. 7. Some misalignments with the ground truth can be seen in particular zones, where the standard techniques tend to enlarge the mask specially on the neck and spinal cord.

We tested the performance of our approach with the database synthetic MRI BrainWeb database contains simulated MR images volumes for normal brain for T1w, T2w and PD images with five degrees of noise were chose for 0% to 40% of intensity non uniformity and MRI Multiple sclerosis Database. The brain images were transformed to the axial, coronal and sagittal orientations before starting experiments. The qualitative results of the simulated brains for axial, coronal and sagittal slices shown in Figs. 10, 11, and 12, respectively, and the quantitative results are presented in Table I and Fig. 9. This validation shows that the results produced by our method (RMBE) are comparable to or better than

TABLE I
THE QUANTITATIVE RESULTS OF OUR APPROACH FOR BRAINWEB DATA SET IN DIFFERENT MODALITIES (PD, T1W, AND T2W) BY SLICES

Modality	Slice	Mean of DSC
PD	Axial	0.965
	Coronal	0.952
	Sagittal	0.918
T1w	Axial	0.972
	Coronal	0.966
	Sagittal	0.964
T2w	Axial	0.902
	Coronal	0.913
	Sagittal	0.898

the popular methods BET[22], BSE[23], MARGA[21] and SPM[32]. Moreover, analyzing the results, we observed that when using the T1-weighted the better DSC was obtained (0.968 ± 0.015) than when using T2-weighted (0.915 ± 0.021). Fig. 8 shows a quantitative comparison between our method with the well-known MARGA, BET, BSE and SPM.

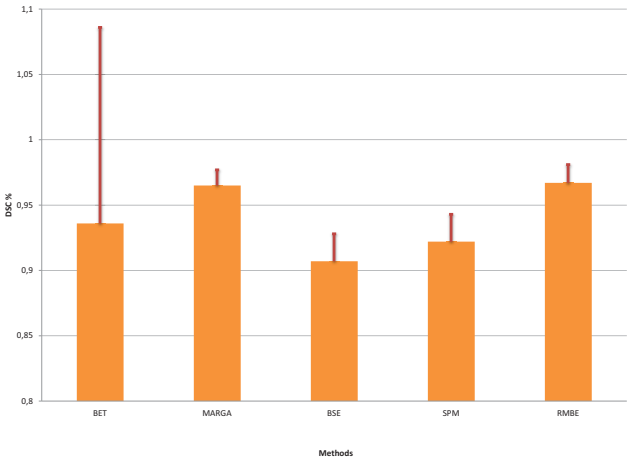

Fig. 8 Quantitative comparison between our method with the well-known algorithms of brain extraction

The proposed approach take full image to start processing, against the well-known methods start from the middle slice. However, other methods use the combination between T1-weighted and T2-weighted to obtain the brain extraction. The existing methods require some preprocessing technique like rotation and cropping. In addition, certain parameters as input to start procedure or others take a specific view of slice. But our method require only the brain boundary detection using the generalized tensor to brain extraction in multi-modal MRI. Another challenge of medical image processing is the time-consuming procedure, being this point some of the existing methods take more time. To evaluate the efficacy of our algorithm, the running time takes $1.6s$ for boundary detection and $2.9s$ for brain segmentation.

VI. CONCLUSION

In this paper, we proposed a new adaptive image segmentation and extraction algorithms, which is based on a Riemannian manifolds, where structure Tensor, geodesic

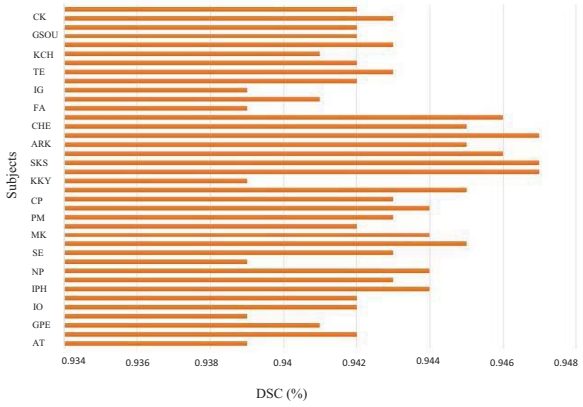

Fig. 9 Average of DSC for brain extraction using the proposed method for MRI Multiple sclerosis Database

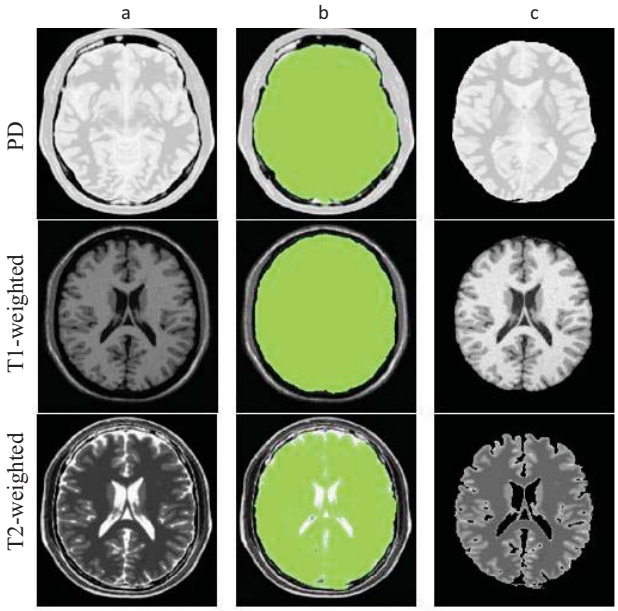

Fig. 10 The steps of the axial slice brain segmentation and extraction based on the Riemannian metric tensor from left to right, (a) original image, (b) brain mask, (c) brain region extracted for the PD, T1w and T2w, respectively from the first line

distance for brain multi-modal MR image segmentation and extraction.

Firstly, our method uses a slice by slice filtering and smoothing of the 3D MRI volumes as residing on a Riemannian manifold and we generalize the approach of [1] used for filtering and edge detection with non-Euclidean image data to segmentation and brain region extraction. This initial pre-treating approach 325 provides a robust brain boundary using a generalized tensor, which ensure the true brain one. Secondly, based on the slice filtering and edge detection the segmentation of the boundary detected using geodesic distance, exponential map and intrinsic metric, carried out.

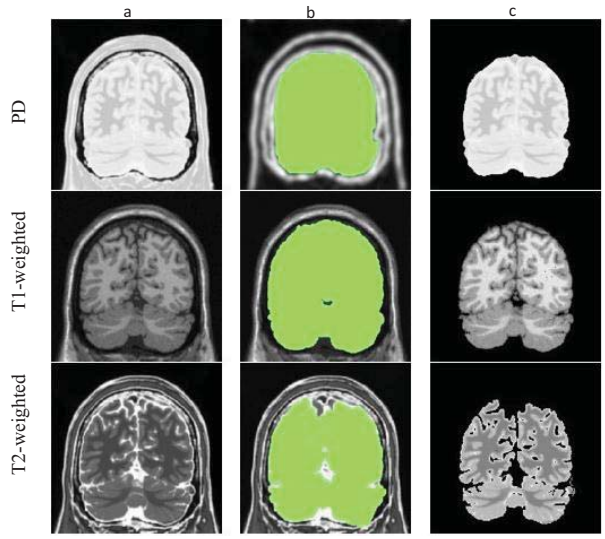

Fig. 11 The steps of the coronal slice segmentation and extraction based on the Riemannian metric tensor from left to right, (a) original image, (b) brain mask, (c) brain region extracted for the PD, T1w and T2w, respectively from the first line

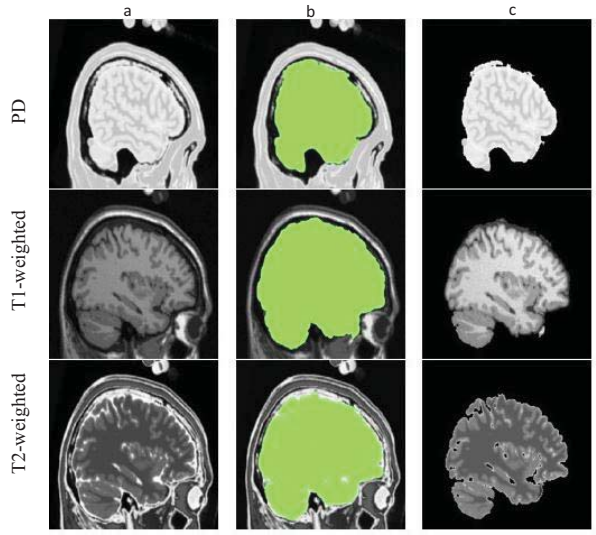

Fig. 12 The steps of the sagittal slice segmentation and extraction based on the Riemannian metric tensor from left to right, (a) original image, (b) brain mask, (c) brain region extracted for the PD, T1w and T2w, respectively from the first line

The generalization investigate the connection between the four neighbours pixels of a region intensity. Qualitative and quantitative results on synthetic and real MR images data illustrate a higher robustness to brain region segmentation and extraction on three modalities T1-weighted, T2-weighted and Proton density on both normal and abnormal slices.

ACKNOWLEDGMENT

We would like to thank deeply Professor Mohamed Naimi, Vice-Dean of Polydisciplinary Faculty of Beni-Mellal, for his precious help.

REFERENCES

[1] F. Zhang and E. R. Hancock, "New riemannian techniques for directional and tensorial image data," *Pattern Recognition*, vol. 43, no. 4, pp. 1590 – 1606, 2010. (Online). Available: http://www.sciencedirect.com/science/article/pii/S0031320309003616

[2] X. Pennec, P. Fillard, and N. Ayache, "A riemannian framework for tensor computing," *International Journal of Computer Vision*, vol. 66, no. 1, pp. 41–66, 2006. (Online). Available: http://dx.doi.org/10.1007/s11263-005-3222-z

[3] P. Thomas Fletcher and S. Joshi, "Riemannian geometry for the statistical analysis of diffusion tensor data," *Signal Processing*, vol. 87, pp. 250–262, 2007.

[4] A. L. Troter, G. Auzias, and O. Coulon, "Automatic sulcal line extraction on cortical surfaces using geodesic path density maps." *NeuroImage*, vol. 61, pp. 941–949, 2012.

[5] X. Hao, K. Zygmunt, R. T. Whitaker, and P. T. Fletcher, "Improved segmentation of white matter tracts with adaptive riemannian metrics." *Medical Image Analysis*, vol. 18, pp. 161–175, 2014.

[6] S. Bak, E. Corve, F. Brmond, and M. Thonnat, "Boosted human re-identification using riemannian manifolds," *Image and Vision Computing*, vol. 30, pp. 443–452, 2012.

[7] S. Barbieri, M. H. Bauer, J. Klein, J. Moltz, C. Nimsky, and H. K. Hahn, "Dti segmentation via the combined analysis of connectivity maps and tensor distances," *NeuroImage*, vol. 60, pp. 1025–1035, 2012.

[8] J. I. Pastore, E. G. Moler, and V. L. Ballarin, "Segmentation of brain magnetic resonance images through morphological operators and geodesic distance," *Digital Signal Processing*, vol. 15, no. 2, pp. 153 – 160, 2005. (Online). Available: http://www.sciencedirect.com/science/article/pii/S1051200404001162

[9] H. Li, Z. Xue, K. Cui, and S. T. Wong, "Diffusion tensor-based fast marching for modeling human brain connectivity network," *Computerized Medical Imaging and Graphics*, vol. 35, no. 3, pp. 167–178, 2011. (Online). Available: http://www.sciencedirect.com/science/article/pii/S0895611110001047

[10] R. Caseiro, P. Martins, J. F. Henriques, and J. Batista, "A nonparametric riemannian framework on tensor field with application to foreground segmentation," *Pattern Recognition*, vol. 45, no. 11, pp. 3997 – 4017, 2012. (Online). Available: http://www.sciencedirect.com/science/article/pii/S0031320312001689

[11] Q. Ain, M. A. Jaffar, and T.-S. Choi, "Fuzzy anisotropic diffusion based segmentation and texture based ensemble classification of brain tumor," *Applied Soft Computing*, vol. 21, no. 0, pp. 330 – 340, 2014. (Online). Available: http://www.sciencedirect.com/science/article/pii/S1568494614001264

[12] L. Astola, A. Fuster, and L. Florack, "A riemannian scalar measure for diffusion tensor images," *Pattern Recognition*, vol. 44, pp. 1885–1891, 2011.

[13] P. Thomas Fletcher, S. Venkatasubramanian, and S. Joshi, "The geometric median on riemannian manifolds with application to robust atlas estimation," *NeuroImage*, vol. 45, pp. S143–S152, 2009.

[14] C. Lopez-Molina, M. Galar, H. Bustince, and B. De Baets, "On the impact of anisotropic diffusion on the edge detection," *Pattern Recognition*, vol. 47, pp. 270–281, 2014.

[15] K. Somasundaram and T. Kalaiselvi, "Fully automatic brain extraction algorithm for axial t2-weighted magnetic resonance images," *Computers in Biology and medicine*, vol. 40, pp. 811–822, 2010.

[16] M. Somasundaram and T. Kalaiselvi, "Automatic brain extraction methods for t1 magnetic resonance images using region labeling and morphological operations," *Computers in Biology and medicine*, vol. 41, pp. 716–725, 2011.

[17] S. F. Eskildsen, P. Coupe, V. Fonov, J. V. Manjon, K. K. Leung, N. Guizard, S. N. Wassef, L. R. stergaard, and D. L. Collins, "Beast brain extraction based on nonlocal segmentation technique," *NeuroImage*, vol. 59, pp. 2362–23–73, 2012.

[18] G. Gilanie, M. Attique, Hafeez-Ullah, S. Naweed, E. Ahmed, and M. Ikram, "Object extraction from t2 weighted brain mr image using histogram based gradient calculation," *Pattern Recognition Letters*, vol. 34, pp. 1356–1363, 2013.

[19] A. H. Foruzan, I. kalantari Khandani, and S. B. Shokouhi, "Segmentation of brain tessues using a 3-d multi-layer hidden markov model," *Computers in Biology and Medicine*, vol. 43, pp. 121–130, 2013.

[20] C. Ballagan, X. Wang, M. Fulham, S. Eberl, and D. dagan Feng, "Lung tumor segmentation in pet images using graph cuts," *Computer Methods and Programs in Biomedicine*, vol. 43, pp. 121–130, 2013.

[21] E. Roura, A. Oliver, M. Cabezas, J. C. Vilanova, lex Rovira, L. Rami-Torrent, and X. Llad, "Marga: Multispectral adaptive region growing algorithm for brain extraction on axial {MRI}," *Computer Methods and Programs in Biomedicine*, vol. 113, no. 2, pp. 655 – 673, 2014. (Online). Available: http://www.sciencedirect.com/science/article/pii/S0169260713003878

[22] S. Smith, "Fast robust automated brain extraction," *Human Brain Mapping*, vol. 17, no. 3, pp. 143–155, 2002.

[23] D. W. Shattuck, S. R. Sandor-Leahy, K. A. Schaper, D. A. Rottenberg, and R. M. Leahy, "Magnetic resonance image tissue classification using a partial volume model," *NeuroImage*, vol. 13, no. 5, pp. 856 – 876, 2001. (Online). Available: http://www.sciencedirect.com/science/article/pii/S1053811900907304

[24] V. Popescu, M. Battaglini, W. Hoogstrate, S. Verfaillie, I. Sluimer, R. van Schijndel, B. van Dijk, K. Cover, D. Knol, M. Jenkinson, F. Barkhof, N. de Stefano, and H. Vrenken, "Optimizing parameter choice for fsl-brain extraction tool (bet) on 3d {T1} images in multiple sclerosis," *NeuroImage*, vol. 61, no. 4, pp. 1484 – 1494, 2012. (Online). Available: http://www.sciencedirect.com/science/article/pii/S1053811912003552

[25] J. G. Park and C. Lee, "Skull stripping based on region growing for magnetic resonance brain images," *NeuroImage*, vol. 47, no. 4, pp. 1394 – 1407, 2009. (Online). Available: http://www.sciencedirect.com/science/article/pii/S1053811909004145

[26] wolfgang Kuhnel, *Differential Geometry: Curves, Surfaces, Manifolds*, 2nd ed. American Mathematical Society, 2006.

[27] S. DiZenzo, "A note on the gradient of a multi-image," *Computer Vision, Graphics,and Image Processing*, vol. 33, pp. 116–125, 1986.

[28] A. G. Weber, "The usc texture mosaic images," *Signal and Image Processing Institute*, 2004.

[29] C. Loizou, V. Murray, M. Pattichis, I. Seimenis, M. Pantziaris, and C. Pattichis, "Multi-scale amplitude modulation-frequency modulation (am-fm) texture analysis of multiple sclerosis in brain mri images," *IEEE Trans. Inform. Tech. Biomed.*, vol. 15, no. 1, pp. 119–129, 2011.

[30] C. Loizou, E. Kyriacou, I. Seimenis, M. Pantziaris, S. Petroudi, M. Karaolis, and C. Pattichis, "Brain white matter lesion classification in multiple sclerosis subjects for the prognosis of future disability,," *Intelligent Decision Technologies Journal (IDT)*, vol. 7, pp. 3–10, 2013.

[31] J.-B. Fiot, L. D. Cohen, P. Raniga, and J. Fripp, "Efficient brain lesion segmentation using multi-modality tissue-based feature selection and support vector machines," *International Journal for Numerical Methods in Biomedical Engineering*, vol. 29, no. 9, pp. 905–915, 2013. (Online). Available: http://dx.doi.org/10.1002/cnm.2537

[32] J. Ashburner and K. J. Friston, "Unified segmentation," *NeuroImage*, vol. 26, no. 3, pp. 839 – 851, 2005. (Online). Available: http://www.sciencedirect.com/science/article/pii/S1053811905001102